

Charged-particle acceleration in braking plasma jets

A. V. Artemyev

Space Research Institute RAS, Moscow, Russia

(Received 27 June 2013; published 27 March 2014)

In this paper we describe the mechanism of the charged particle acceleration in space plasma systems. We consider the interaction of nonrelativistic particles with a sub-Alfvénic plasma jet originated from the magnetic reconnection. The sharp front with increased magnetic field amplitude forms in the jet leading edge. Propagation of the jet in the inhomogeneous background plasma results in front braking. We show that particles can interact with this front in a resonance manner. Synchronization of particle reflections from the front and the front braking provides the stable trapping of particles in the vicinity of the front. This trapping supports the effective particle acceleration along the front. The mechanism of acceleration is potentially important due to the prevalence of the magnetic reconnection in space and astrophysical plasmas.

DOI: [10.1103/PhysRevE.89.033108](https://doi.org/10.1103/PhysRevE.89.033108)

PACS number(s): 52.20.Dq, 52.35.Vd, 94.30.Lr

I. INTRODUCTION

Modern *in situ* spacecraft observations in the near-Earth plasma environment [1,2], numerical models [3,4], and indirect observations in the solar corona [5] suggest that the transient magnetic reconnection releases some portion of the stored magnetic field energy in a form of plasma jets with sharp fronts. These fronts are characterized by the strong increase of the magnetic field amplitude and propagate with a sub-Alfvénic velocity. Jets with distinguished fronts were found in the Earth [6], Jupiter [7], and Mercury [8] magnetospheres owing to various spacecraft missions. Interaction of jets with the surrounding plasma medium results in charged particle acceleration [9–12]. The primary region of this acceleration is the jet front [13].

For the magnetic reconnection region located in planetary magnetotails or in the solar corona, the propagation of plasma jets away from the X-line corresponds to the front motion towards the planet (or towards the initial corona magnetic loop). Eventually, the plasma jet should be stopped by the increased background magnetic field—so-called jet breaking [14]. Thus, there is a certain region where the velocity of front propagation is decreasing (see recent statistics in papers [15,16]). In this paper we show that such front braking (slowing down) gives rise to a new resonance mechanism of the charged particle acceleration. This mechanism resembles the classical shock drift acceleration [17], however, it is more effective in comparison with the drift acceleration. Because of the front braking, the particle reflections from the front can be synchronized with the decrease of the front velocity. In this case, particles do not cross the front and move with it—this is resonant interaction. Thus, particles are trapped by the front similarly with the classical surfatron trapping [18,19]. The magnetic field gradient at the front supports the charged particle drift along the front, i.e., along the convection electric field corresponding to the front motion. As a result, trapped particles can stably gain energy ahead of the front until their reflections are synchronized with the front propagation. This synchronization is impossible for fronts with a constant velocity of propagation. Therefore, we propose the mechanism of resonant particle acceleration.

The system configuration includes the moving front [see Fig. 1(a)] and the inhomogeneous background magnetic field.

The front is characterized by the sharp increase of the B_z component of the magnetic field. The front propagates along the x direction with the velocity $\hat{v}_\phi(x)$. The background magnetic field has one component B_z , which increases with x . The full magnetic field configuration includes the background $B_x(z)$ component, which reverses at the $z = 0$ plane and increases with $|z|$ [13]. We assume that charged particles are trapped between corresponding mirror points located below and above the plane $z = 0$, thus, one can consider the system averaged over particle bounce oscillations [20,21]. This simplified consideration allows us to directly describe the new mechanism of the particle acceleration without introducing additional invariants of motion.

II. ANALYTICAL ESTIMATES

The magnetic field of the simplified configuration includes only one component B_z , which can be written as a sum of the background field $B_0(x/L_x)$ and the front field $B_f(x/L_x)f(\phi)$ (here L_x is the spatial scale of system inhomogeneity along the x direction). The function $f(\phi)$ determines the front structure and dynamics, while the phase ϕ is

$$\phi = \frac{1}{L_f} \int_{L_x}^x \ell(x'/L_x) dx' - \frac{v_\phi t}{L_f} + \phi_0, \quad (1)$$

where ϕ_0 is an initial phase, L_f is the front thickness, v_ϕ is the initial front velocity, and $\ell(x/L_x)$ is the dimensionless function determining evolution of the effective front velocity $\hat{v}_\phi(x) = v_\phi/\ell(x/L_x)$. We consider the space domain $x/L_x > 1$ with $\ell(1) = 1$. Because the dynamical evolution of the front is poorly studied, we choose the phase ϕ similar to a phase of waves propagating in the inhomogeneous medium [22]. Thus, we keep the effective wave-frequency constant $v_\phi/L_f = \text{const}$ and vary the effective wave-number $\ell(x)/L_f$. This is not unique approach to describe the evolution of the front, but we suggest that this approach is quite reasonable and simple.

The convection electric field has the single component $E_y(x/L_x, \phi)$. We assume that E_y can be written as $E_y = E_f(x/L_x)f(\phi)$. The function $E_f(x/L_x)$ can be determined from the Maxwell equation $\partial E_y/\partial x = -c^{-1}(\partial B_z/\partial t)$:

$$f(\phi) \frac{\partial E_f}{\partial x} + E_f \frac{\partial f(\phi)}{\partial \phi} \frac{\partial \phi}{\partial x} = -\frac{1}{c} \frac{\partial \phi}{\partial t} B_f \frac{\partial f(\phi)}{\partial \phi}. \quad (2)$$

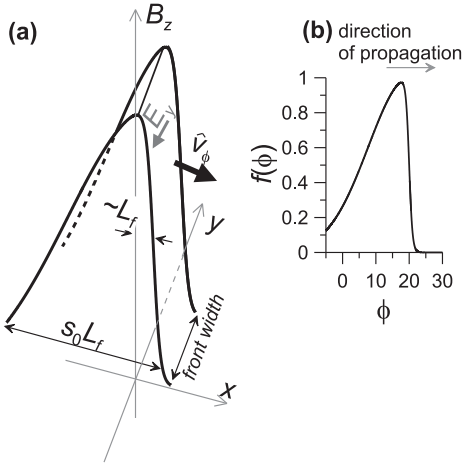


FIG. 1. Schematic view of the system (a). Profile of the $f(\phi)$ function (b).

Comparison of two terms in the left-hand side of this equation gives

$$\frac{f}{E_f} \frac{\partial E_f}{\partial x} \left(\frac{\partial f}{\partial \phi} \frac{\partial \phi}{\partial x} \right)^{-1} \sim \frac{L_f}{L_x}. \quad (3)$$

Thus, we can omit the first term when the front thickness L_f is much smaller than the inhomogeneity scale of the magnetic field variation L_x ($L_f \ll L_x$). This approximation substantially simplifies the final expression for the convection electric field: $E_y \approx (\hat{v}_\phi/c) B_f(x/L_x) f(\phi)$. Moreover, for the particular case of $B_f \sim \ell(x)$ our approximation provides the exact expression for E_y (in this case $E_f \sim \hat{v}_\phi B_f$ does not depend on x).

Dimensionless profiles of front magnetic and electric fields are shown for three moments of time in Fig. 2. With time the leading edge of the front becomes more sharp (here we

use $\ell \sim x^\alpha$ and $B_f \sim \ell^\sigma$). For constant B_f (i.e., for $\sigma = 0$) the electric field amplitude decreases during front propagation $E_f \sim B_f/\ell \sim \ell^{-1}$. For growing $B_f \sim \ell$ (i.e., for $\sigma = 1$) the electric field amplitude is constant $E_f \sim B_f/\ell \sim \text{const}$.

For the simplified system with $B_f = \text{const}$, $\ell = \text{const}$, several models with various functions $f(\phi)$ were considered before: $f(\phi) = \sin \phi$ [23,24], $f(\phi) = \tanh(\phi)$ [9,25], $f(\phi) = \phi \exp(-(\phi + \phi_0)^2)$ [26]. Here we use $f(\phi) = (1/2)(1 - \tanh \phi) \exp(-\phi^2/s_0)$ with $s_0 = 100$ [see Fig. 1(b)]. This model describes all the main properties of observed fronts [6]: 1) the sharp increase of the magnetic field in the front (the small value of L_f), 2) the weak gradient behind the front ($s_0 \gg 1$). We assume that the front has a finite size along the y direction in agreement with spacecraft observations [27].

In contrast to the previous models [20,25,26] the function $f(\phi)$ is positive for all ϕ values [see Figs. 1(b), 2]. The magnetic surfatron [20,24] (or magnetic trapping [25]) mechanism of the charged particle acceleration cannot be realized in the system with $f(\phi) > 0$ because this mechanism requires the presence of magnetic field nulls [$B_0 + B_f f(\phi) = 0$] [23]. Moreover, we do not include any electrostatic fields which can be responsible for the classical surfatron acceleration [28–30]. Thus, we consider an acceleration mechanism different from the surfatron.

We describe an interaction of the front and a nonrelativistic ion with the charge q and the mass m . Corresponding equations of motion can be written as

$$\begin{aligned} \dot{v}_x &= v_y(\Omega_0(x) + \Omega_f(x)f(\phi)) \\ \dot{v}_y &= \hat{v}_\phi(x)\Omega_f(x)f(\phi) - v_x(\Omega_0(x) + \Omega_f(x)f(\phi)) \end{aligned} \quad (4)$$

where $\{v_x, v_y\}$ are components of the particle velocity (we do not take into account the particle motion along the z direction, because the system is z averaged), $\Omega_0(x) = qB_0(x)/mc$, $\Omega_f(x) = qB_f(x)/mc$. In the vicinity of the Cherenkov resonance, $v_x = \hat{v}_\phi(x)$ two terms $\sim \Omega_f(x)$ in the

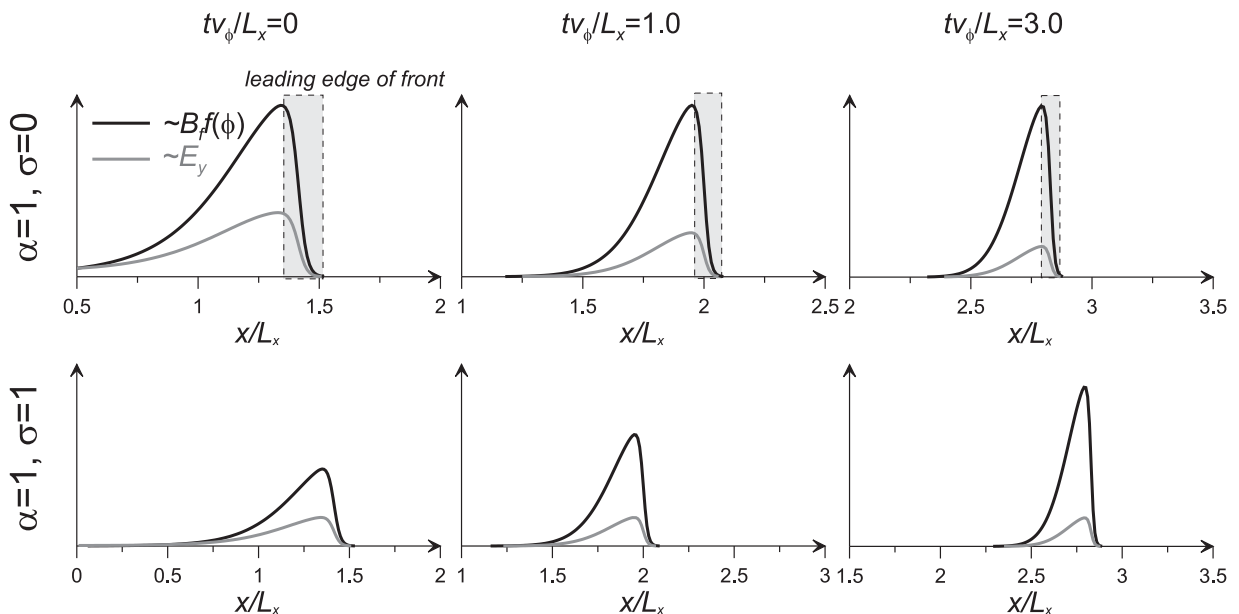


FIG. 2. Magnetic field profiles $B_f(x/L_x)f(\phi)$ for two values of σ and three time moments. We take $L_x/L_f = 20$ and $s_0 = 10$ for illustration. Grey area shows the leading edge of fronts where $df/d\phi < 0$.

second equation (4) are canceled out and we can rewrite this system as

$$\begin{aligned} d\hat{v}_\phi/dt &= v_y(\Omega_0(x) + \Omega_f(x)f(\phi)) \\ \dot{v}_y &= -\hat{v}_\phi(x)\Omega_0(x) \end{aligned} \quad (5)$$

The second equation can be integrated with $d/dt = \hat{v}_\phi(x)d/dx$. Thus, we can write the condition of resonant interaction of particles with the front:

$$\begin{aligned} \hat{v}_\phi(x) \frac{d\hat{v}_\phi(x)}{dx} &= \left(\text{const} - \int_{x_0}^x \Omega_0(x') dx' \right) \\ &\times (\Omega_0(x) + \Omega_f(x)f(\phi)), \end{aligned} \quad (6)$$

where $dv_y/dx = -\Omega_0(x)$. For the surfatron mechanism in a homogeneous field ($d\hat{v}_\phi/dx = 0$) this resonant condition can be satisfied only if $\Omega_0 + \Omega_f f(\phi) = 0$ for some ϕ value [20,25] or if there is an additional term in the right-hand side of Eq. (6) corresponding to an electrostatic field [28–30]. However, here we consider the new mechanism when the resonant condition (6) is satisfied due to $d\hat{v}_\phi/dx \neq 0$ for $\Omega_0 + \Omega_f f(\phi) > 0$.

We introduce simple functions to describe the system inhomogeneity along the x direction: $\Omega_0(x) = \bar{\Omega}_0 \ell^\sigma(x)$, $\Omega_f(x) = \bar{\Omega}_f \ell^\sigma(x)$, and $\ell(x) = (x/L_x)^\alpha$, where $\bar{\Omega}_0$, $\bar{\Omega}_f$, α , σ are constants. At this time spacecraft observations and numerical modelings (e.g., [12,31]) cannot give any clear information about how \hat{v}_ϕ depends on the magnetic field inhomogeneity σ . Thus, we consider both scenarios: the front braking (the decrease of \hat{v}_ϕ with x) in the homogeneous magnetic field with $\sigma = 0$ and the front braking in the inhomogeneous magnetic field with $\sigma \neq 0$. The first scenario is simpler for analytical estimates, while the second scenario is more realistic. For the second scenario the amplitude of the convection electric field $\hat{v}_\phi(x)B_f(x) \sim \ell^{\sigma-1}$ grows with x for $\sigma > 1$. For the first scenario $\hat{v}_\phi(x)B_f(x)$ decreases with x (see Fig. 2).

Resonance condition (6) can be rewritten as

$$f(\phi) = \frac{\bar{\Omega}_0}{\bar{\Omega}_f} (r^2 \alpha (1 + \sigma \alpha) \ell^{-2(1+\alpha+\sigma\alpha)/\alpha} - 1), \quad (7)$$

where $r = v_\phi/(\bar{\Omega}_0 L_x)$ and we choose x_0 to remove the constant term in Eq. (6). If Eq. (7) has a solution ϕ^* then particles can be captured into the resonance. The function $f(\phi)$ is positive and less than one. Thus, we can determine the spatial domain where the resonance condition is satisfied [i.e., where Eq. (7) has a solution]: $\ell_{\min} < \ell < \ell_{\max}$ with

$$\begin{aligned} \ell_{\max} &= r^{\alpha/(1+\alpha+\sigma\alpha)} (\alpha(1 + \sigma\alpha))^{\alpha/(2+2\alpha+2\sigma\alpha)}, \\ \times \ell_{\min} &= \ell_{\max} \left(\frac{\bar{\Omega}_f}{\bar{\Omega}_0} + 1 \right)^{-\alpha/(2+2\alpha+2\sigma\alpha)}. \end{aligned} \quad (8)$$

The latter condition $\ell > \ell_{\min}$ is satisfied for a large enough front amplitude ($\bar{\Omega}_f \gg \bar{\Omega}_0$). The condition $\ell < \ell_{\max}$ determines the maximum possible gain of energy. We can write the following expression for the v_y component of the particle velocity in the resonance:

$$v_y/v_\phi = -\frac{1}{r} \frac{\ell^{(1+\sigma\alpha)/\alpha}}{1 + \sigma\alpha}. \quad (9)$$

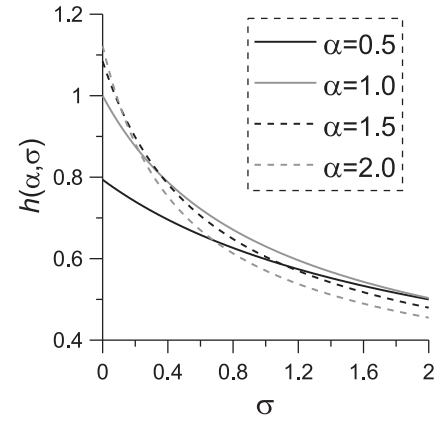


FIG. 3. Profiles of $h(\alpha, \sigma)$ function for four values of α .

Therefore, we obtain estimates of the maximum value of $|v_y|$:

$$\begin{aligned} \max |v_y/v_\phi| &< r^{-\alpha/(1+\alpha+\sigma\alpha)} h(\alpha, \sigma) \\ h(\alpha, \sigma) &= \frac{\alpha^{(\alpha\sigma+1)/(2+2\alpha+2\sigma\alpha)}}{(1 + \sigma\alpha)^{(1+2\alpha+\sigma\alpha)/(2+2\alpha+2\sigma\alpha)}}. \end{aligned} \quad (10)$$

Function h decreases with σ (see Fig. 3) and for fixed α the acceleration is the most effective for $\sigma \rightarrow 0$. For example, in the Earth magnetotail we have $L_x \sim 2 - 10R_E$ [15,16], where $R_E \approx 6400$ km is the Earth radius. The amplitude of the front velocity is within the range $v_\phi \sim 500-1500$ km/s, and the amplitude of the background magnetic field is $B_0 \sim 1-10$ nT. Corresponding estimates for $\alpha = 1$ and $\sigma = 0$ gives the maximum proton energy $\sim \max |v_y|^2$ from ten keV up to a few hundred keV km/s (see Fig. 4). For moderate values of $v_\phi \sim 500$ km/s protons can gain 10–100 keV. This gain of energy is comparable with the spacecraft observations (see [12,13] and references therein).

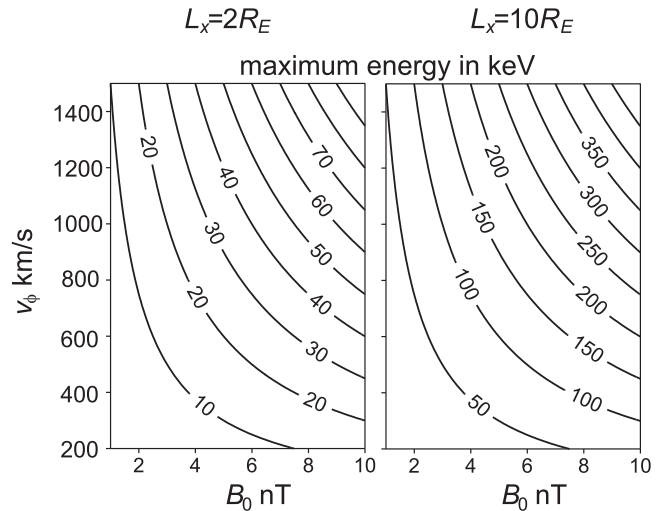


FIG. 4. Maximum energy gained by protons due to resonant acceleration $\sim \max |v_y|^2$ is shown as a function of system parameters.

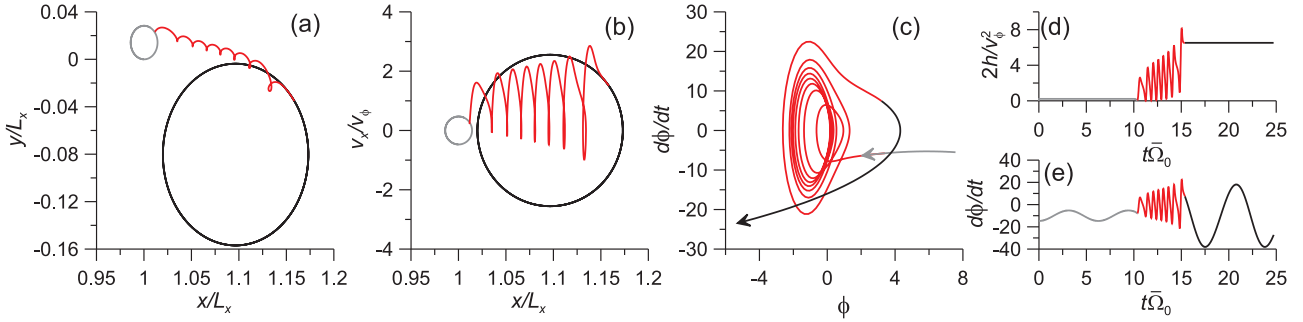


FIG. 5. (Color online) The particle trajectory is shown in the (x, y) plane (a) and in the (x, v_x) plane (b). The fragment of the particle trajectory in the trapping is shown in the $(\phi, d\phi/dt)$ plane (c). The particle energy and $d\phi/dt$ as functions of time are shown in (d), (e). Grey and black colors are used for fragments before the trapping and after the escape from the resonance, while the red color shows the fragment of the trapped motion. System parameters are $L_x = 100\rho_0$, $v_\phi = 3v_0$, $L_f = 0.3\rho_0$, $\alpha = 1$, $\sigma = 0$, where the initial particle energy is $H = v_0^2/2$ and the initial particle Larmor radius is $\rho_0 = v_0/\Omega_0$. The front magnetic field is nonzero only for $y/\rho_0 \in [-5, 5]$. For the typical conditions in the Earth magnetotail $\rho_0 \sim 1000\text{--}2000$ km and, thus, we have $|y| < 10^4$ km in agreement with spacecraft observations [27].

III. NUMERICAL SIMULATIONS

To demonstrate particle dynamics in the resonance we solve system (4) numerically. We start with the simplest case of homogeneous magnetic field $\sigma = 0$. Figure 5(a) shows the typical particle trajectory: grey and black colors are used for the initial (before the trapping) and the final (after the escape) Larmor rotations corresponding to the particle motion in the background magnetic field. The red color shows the fragment of the trajectory when the particle moves with the front and gains energy due to the drift along the front. In the (x, y) plane the particle trajectory looks like two Larmor circles connected by the resonant fragment. The resonant particle reflects from the front several times, while the front transports this particle along the x direction. As a result, the resonant fragment of the trajectory (red curve) is a combination of the motion in the x direction with the front velocity $\hat{v}_\phi(x)$ and the drift motion in the $-y$ direction.

Figure 5(b) demonstrates the same trajectory in the (x, v_x) plane. One can see that the particle resonant motion is characterized by v_x oscillations around the value of the front velocity, i.e., $v_x/v_\phi \sim 1$. This is the classical phase trapping picture, which can be confirmed also by Fig. 5(c): the particle quasiperiodically oscillates in the plane $(\phi, d\phi/dt)$. Oscillations of $d\phi/dt$ around zero value (i.e., the particle motion with the front) are well seen in Figs. 5(c), (e). These quasiperiodical oscillations correspond to the particle acceleration [see Fig. 5(d) where the particle energy $H = (v_x^2 + v_y^2)/2$ is shown]. The particle energy oscillates, but the amplitude of these oscillations increases. After the particle escape from the resonance, the energy is substantially larger than the initial value.

Effects of the inhomogeneity of the background magnetic field ($\sigma \neq 0$) on the particle acceleration are demonstrated in Fig. 6. We show particle trajectories in the (x, y) and (v_x, v_y) planes. Red color indicates fragments of the resonant (trapped) motion. The increase of α and a nonzero value of σ slightly modify trajectories. Here we consider the front with a finite width in the y direction. Thus, particles escape from the resonance around the front boundary and the corresponding final energy is determined by the front width. This energy is smaller than estimates given by Eq. (10) for all used values σ

and α . As a result, the final energy is approximately the same for all three examples with different σ shown in Fig. 6. Effects of the magnetic field configuration ($\sigma \neq 0$) may play a more

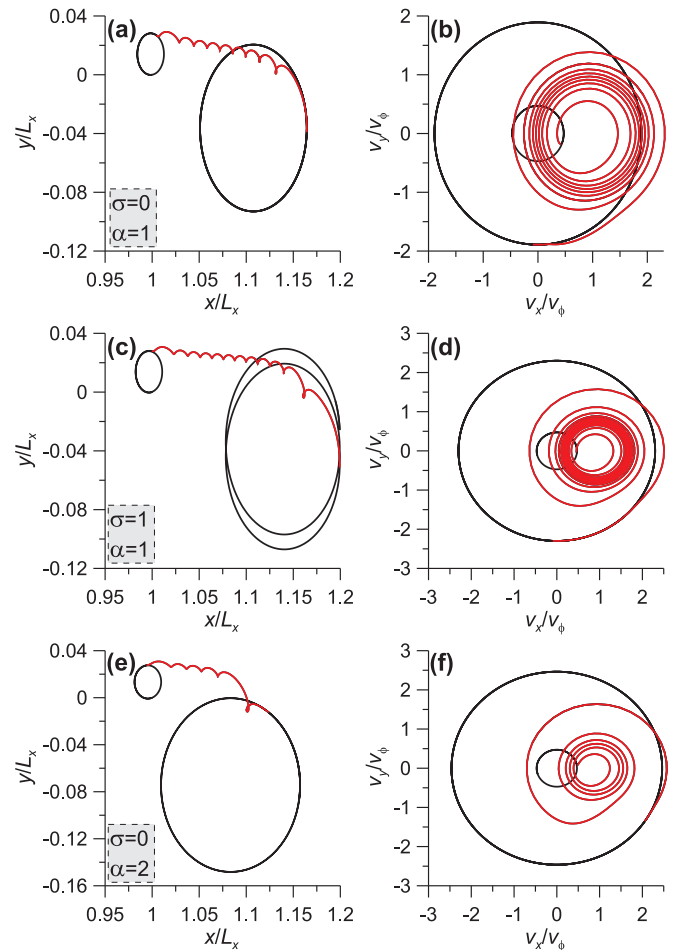


FIG. 6. (Color online) Three particle trajectories are shown in the (x, y) plane (a,c,e) and in the (v_x, v_y) plane (b,d,f). The black color is used for fragments before the trapping and after the escape, while the red color shows the fragment of the trapped motion. System parameters are the same as in Fig. 5.

important role and determine the final energy for wide enough fronts. However, in this case the classical mechanism of the particle drift acceleration may be important as well [17,21]. An investigation of effects of front breaking on the particle nonresonant drift acceleration is beyond the scope of this paper. We can conclude that for narrow enough fronts the inhomogeneity of the background magnetic field does not substantially change the character of the resonant particle motion.

Trapped particles move along the untwisted spiral in the (v_x, v_y) plane (see right panels in Fig. 6). This is drastically different from the classical motion of trapped particles when only the v_x component oscillates, while the v_y component grows due to acceleration along the front (the surfatron acceleration, e.g., [19]). Obtained particle trajectories resemble trajectories of particles trapped by a circular wave into the gyrosurfatron regime of acceleration [32]. Trapped particles are reflected from the front and cannot cross it due to the front braking. Thus, we would rather deal with the gyroresonance acceleration than with the classical Landau resonance describing the surfatron mechanism [19,24].

A resonant interaction of particles with braking front corresponds to the decrease of the front velocity \hat{v}_ϕ and, as a result, the averaged value of v_x also should decrease. However, trajectories shown in Figs. 5 and 6 in the (v_x, v_y) plane have such large amplitudes of oscillations of the v_x component that this decrease of averaged v_x cannot be seen. To show that the resonant velocity indeed decreases we plot separately the v_x component as a function of time in Fig. 7. The blue curve shows \hat{v}_ϕ along the trajectory. Before the resonant trapping and after the escape from the resonance (shown by dotted curves) the velocity \hat{v}_ϕ oscillates with the x coordinate of the gyrorotating particle. In the resonance we can clearly see that \hat{v}_ϕ calculated along the trajectory decreases (see the bottom panel of Fig. 7), while the v_x component oscillates around \hat{v}_ϕ .

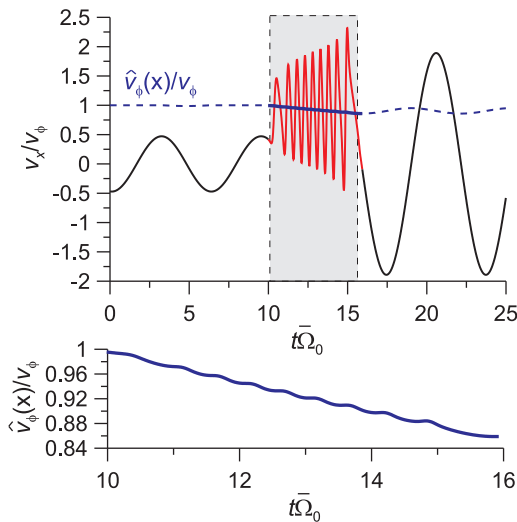


FIG. 7. (Color online) The dependence of v_x on time is shown with the $\hat{v}_\phi(x)$ profile (in blue) for the trajectory presented in top panels of Fig. 6. Fragment of $\hat{v}_\phi(x)$ variation along the trajectory in the resonance (indicated by grey color in the top panel) is shown in the bottom panel.

Besides the resonant acceleration, there is a simple reflection of particles from the front with an energy gain [9,17,21]. To compare these two mechanisms (the resonant acceleration of trapped particles and the nonresonant reflection) we numerically integrate 10^6 trajectories with the same initial energy and plot the final energy distribution in Fig. 8. The energy distribution consists in two parts: 1) the small energy part ($2h < 5v_\phi^2$) corresponds to particle reflection from the front and 2) the high-energy tail ($2h > 5v_\phi^2$) contains particles accelerated by the resonant mechanism [see typical trajectories (a) and (b) in Fig. 8]. The boundary between these two populations in the energy space is not very distinctive because trajectories of resonant particles with only one period of oscillations look very similar to trajectories of reflected particles. Thus, we can only guarantee that particles with $2h > 5.5v_\phi^2$ are really accelerated by a resonant mechanism, while particles with $2h \sim 5v_\phi^2$ can be accelerated by both resonant and nonresonant mechanisms. Figure 8 shows that the resonant interaction allows particles to gain larger energy in comparison to the energy gained by reflected particles. However, the resonance is available only for particles with certain (resonant) velocities and, as a result, the population of high-energy particles is substantially smaller than the population of particles accelerated via nonresonant reflections.

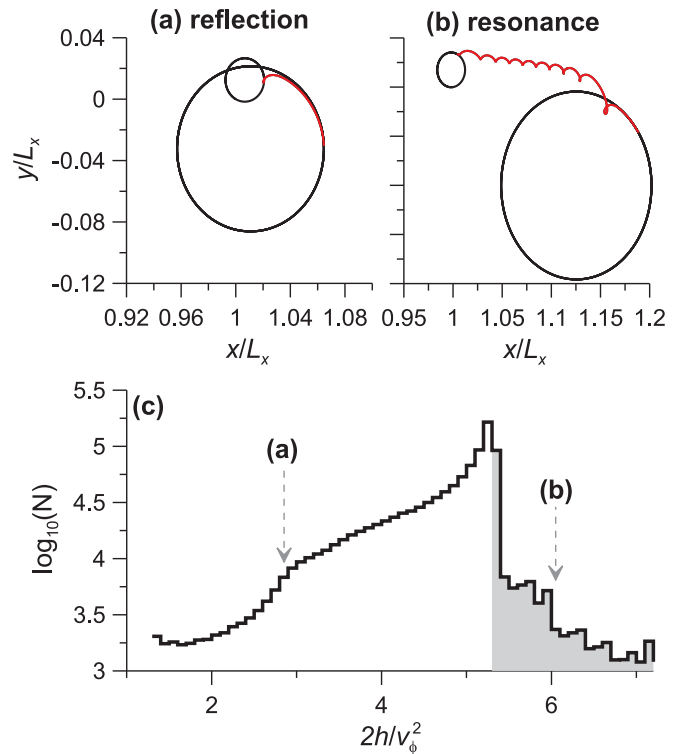


FIG. 8. (Color online) (a) and (b) show two particle trajectories. The black color is used for fragments before the trapping and after the escape, while the red color shows the fragment of the trapped motion. (c) shows the energy distribution for the particle ensemble (the total number of particles is 10^6). The grey color indicates the tail of the distribution containing resonantly accelerated particles. System parameters are the same as in Fig. 5.

IV. DISCUSSION AND CONCLUSIONS

In this paper we consider the new mechanism of the charged particle acceleration by the braking front of the plasma jet. This mechanism can be realized in many plasma systems where sub-Alfvénic jets are formed by magnetic reconnection outflows [3,5,33]. Regular observations of such jets in the Earth magnetotail [31,34,35] suggest that the proposed mechanism of acceleration can be effective. For example, the braking of plasma jets in the close vicinity of the Earth geostationary orbit is always accompanied by the significant increase of fluxes of high-energy (~ 100 keV) ions [13]. The proposed mechanism can be responsible for the local ion acceleration in this region. Models and spacecraft observations show that almost all reconnection events in the magnetotail should result in the formation of plasma jets with corresponding fronts [3,33]. Thus, the resonant acceleration on fronts seems to be as widespread in planetary magnetotails as the acceleration in reconnection regions. For plasma jets originating from reconnection regions in solar wind [36] the proposed mechanism can be even more important owing to larger spatial scales of fronts. Moreover, the recent numerical modeling points to possible spontaneous (without the magnetic reconnection) formation of plasma jet fronts in the specific magnetic field configurations realized in the magnetotail [4]. Thus, the resonant acceleration of particles by fronts can be realized even in the absence of the magnetic reconnection.

It is worth noting one additional possible application of the proposed mechanism of charged particle acceleration. Recent observations of γ -ray bursts in the Crab nebula gave rise to growing investigations of the role of the magnetic reconnection in producing of high-energy particles in the pulsar magnetospheres [37]. One of the perspective scenarios of such acceleration includes interaction of plasma jets with shock waves [38]. This interaction assumes the plasma jet breaking, thus, conditions for the resonant acceleration can be satisfied.

In conclusion, we propose the new resonant mechanism of charged particle acceleration by braking fronts of plasma jets. We show that the resonant acceleration is more effective than the nonresonant acceleration via particle reflections. In the case of the resonant acceleration, the particle motion resembles the gyroresonant motion. The gained energy depends on the front configuration (width), on the magnetic field inhomogeneity (σ), and on the rate of front braking (α).

ACKNOWLEDGMENTS

The author is thankful to V. Krasnoselskikh (LPC2E) and V. A. Sergeev (SPbSU) for fruitful discussions. This work was partially supported by the Program (OFN-15) of the Division of Physical Sciences of the Russian Academy of Sciences.

-
- [1] V. Angelopoulos, A. Runov, X. Z. Zhou, D. L. Turner, S. A. Kiehas, S. S. Li, and I. Shinohara, *Science* **341**, 1478 (2013).
 - [2] H. S. Fu, J. B. Cao, Y. V. Khotyaintsev, M. I. Sitnov, A. Runov, S. Y. Fu, M. Hamrin, M. André, A. Retinò, Y. D. Ma, H. Y. Lu, X. H. Wei, and S. Y. Huang, *Geophys. Res. Lett.* **40**, 6023 (2013).
 - [3] M. I. Sitnov and M. Swisdak, *J. Geophys. Res.* **116**, A12216 (2011).
 - [4] M. I. Sitnov, N. Buzulukova, M. Swisdak, V. G. Merkin, and T. E. Moore, *Geophys. Res. Lett.* **40**, 22 (2013).
 - [5] S. Takasao, A. Asai, H. Isobe, and K. Shibata, *Astrophys. J. Lett.* **745**, L6 (2012).
 - [6] A. Runov, V. Angelopoulos, M. I. Sitnov, V. A. Sergeev, J. Bonnell, J. P. McFadden, D. Larson, K. Glassmeier, and U. Auster, *Geophys. Res. Lett.* **36**, L14106 (2009).
 - [7] S. Kasahara, E. A. Kronberg, N. Krupp, T. Kimura, C. Tao, S. V. Badman, A. Retinò, and M. Fujimoto, *J. Geophys. Res.* **116**, A11219 (2011).
 - [8] T. Sundberg, J. A. Slavin, S. A. Boardsen, B. J. Anderson, H. Korth, G. C. Ho, D. Schriver, V. M. Uritsky, T. H. Zurbuchen, J. M. Raines, D. N. Baker, S. M. Krimigis, R. L. McNutt, Jr., and S. C. Solomon, *J. Geophys. Res.* **117**, A00M03 (2012).
 - [9] X.-Z. Zhou, V. Angelopoulos, V. A. Sergeev, and A. Runov, *J. Geophys. Res.* **115**, A00I03 (2010).
 - [10] M. Ashour-Abdalla, M. El-Alaoui, M. L. Goldstein, M. Zhou, D. Schriver, R. Richard, R. Walker, M. G. Kivelson, and K.-J. Hwang, *Nature Physics* **7**, 360 (2011).
 - [11] H. S. Fu, Y. V. Khotyaintsev, A. Vaivads, A. Retinò, and M. André, *Nature Phys.* **9**, 426 (2013).
 - [12] J. Birn, M. Hesse, R. Nakamura, and S. Zaharia, *J. Geophys. Res.* **118**, 1960 (2013).
 - [13] J. Birn, A. V. Artemyev, D. N. Baker, M. Echim, M. Hoshino, and L. M. Zelenyi, *Space Sci. Rev.* **173**, 49 (2012).
 - [14] Y. V. Khotyaintsev, C. M. Cully, A. Vaivads, M. André, and C. J. Owen, *Phys. Rev. Lett.* **106**, 165001 (2011).
 - [15] V. A. Sergeev, I. A. Chernyaev, V. Angelopoulos, A. V. Runov, and R. Nakamura, *Geophys. Res. Lett.* **41**, 1106 (2014).
 - [16] J. Liu, V. Angelopoulos, X.-Z. Zhou, and A. Runov, *J. Geophys. Res.: Space Physics* **119**, 909 (2014).
 - [17] R. B. Decker, *Space Sci. Rev.* **48**, 195 (1988).
 - [18] R. Z. Sagdeev, *Reviews of Plasma Physics*, 1st ed., Vol. 4 (Consultants Bureau, New York, 1966).
 - [19] T. Katsouleas and J. M. Dawson, *Phys. Rev. Lett.* **51**, 392 (1983).
 - [20] A. V. Artemyev, S. Kasahara, A. Y. Ukhorskiy, and M. Fujimoto, *Plan. Sp. Sci.* **82–83**, 134 (2013).
 - [21] A. Y. Ukhorskiy, M. I. Sitnov, V. G. Merkin, and A. V. Artemyev, *J. Geophys. Res.* **118**, 4952 (2013).
 - [22] V. L. Ginzburg and A. A. Rukhadze, *Waves in Magnetoactive Plasma*, 2nd ed. (Nauka, Moscow, 1975).
 - [23] S. Takeuchi, K. Sakai, M. Matsumoto, and R. Sugihara, *Phys. Lett. A* **122**, 257 (1987).
 - [24] A. I. Neishtadt, A. V. Artemyev, L. M. Zelenyi, and D. L. Vainshtein, *JETP Lett.* **89**, 441 (2009).
 - [25] S. Takeuchi, *Phys. Plasmas* **12**, 102901 (2005).

- [26] A. V. Artemyev, V. N. Lutsenko, and A. A. Petrukovich, *Ann. Geophys.* **30**, 317 (2012).
- [27] R. Nakamura, W. Baumjohann, C. Mouikis, L. M. Kistler, A. Runov, M. Volwerk, Y. Asano, Z. Vörös, T. L. Zhang, B. Klecker, H. Rème, and A. Balogh, *Geophys. Res. Lett.* **31**, L09804 (2004).
- [28] M. Gedalin, *J. Geophys. Res.* **101**, 4871 (1996).
- [29] M. A. Lee, V. D. Shapiro, and R. Z. Sagdeev, *J. Geophys. Res.* **101**, 4777 (1996).
- [30] M. Hoshino, *J. Geophys. Res.* **110**, 10215 (2005).
- [31] A. Runov, V. Angelopoulos, X.-Z. Zhou, X.-J. Zhang, S. Li, F. Plaschke, and J. Bonnell, *J. Geophys. Res.* **116**, A05216 (2011).
- [32] Y. Kuramitsu and V. Krasnoselskikh, *Phys. Rev. Lett.* **94**, 031102 (2005).
- [33] A. Runov, V. Angelopoulos, and X.-Z. Zhou, *J. Geophys. Res.* **117**, A05230 (2012).
- [34] D. Schmid, M. Volwerk, R. Nakamura, W. Baumjohann, and M. Heyn, *Ann. Geophys.* **29**, 1537 (2011).
- [35] H. S. Fu, Y. V. Khotyaintsev, A. Vaivads, M. André, and S. Y. Huang, *Geophys. Res. Lett.* **39**, L10101 (2012).
- [36] J. T. Gosling, S. Eriksson, R. M. Skoug, D. J. McComas, and R. J. Forsyth, *Astrophys. J.* **644**, 613 (2006).
- [37] J. Arons, *Space Sci. Rev.* **173**, 341 (2012).
- [38] L. Sironi and A. Spitkovsky, *Astrophys. J.* **741**, 39 (2011).